Application of independent component analysis to dynamic contrast-enhanced imaging for assessment of cerebral blood perfusion

X.Y. Wu [a,b,*], G.R. Liu [a,c]

[a] *Centre for Advanced Computations in Engineering Science, National University of Singapore, BLK EA-04-26, 10 Kent Ridge Crescent, Singapore 119260, Singapore*
[b] *Institute of Engineering Science, National University of Singapore, University Hall, #UHL-05, Lee Kong Chian wing, 21 Lower Kent Ridge Road, Singapore 119077, Singapore*
[c] *Mechanical Engineering Department, National University of Singapore, 9 Engineering Drive 1, Singapore 117576, Singapore*

Abstract

Dynamic contrast-enhanced (DCE) imaging is widely used for in vivo assessment of the cerebral blood perfusion. In this work, we investigate the use of independent component analysis (ICA) on DCE imaging data for assessment of cerebral blood perfusion, without any prior knowledge of the underlying tissue vasculature and arterial input function. The minimum description length (MDL) criterion and principle component analysis (PCA) were employed to reduce the dimension of the data. An oscillating index method was used to select the components of interest. Numerical simulation and patient case studies were carried out to investigate the performance of ICA. The results show that ICA is able to extract physiologically meaningful components from the DCE imaging data. The advantages of ICA include its efficiency of computation, clarity of obtained component maps, and no need of the manually selected input function. The obtained independent component maps can provide reliable reference to identify the arterial and venous structure, and allow better demarcation of the tumor territories. The potential of ICA to be a useful clinical tool for diagnosis of cerebral vascular disease and for the assessment of treatment response has been demonstrated.
© 2007 Elsevier B.V. All rights reserved.

Keywords: Independent component analysis; Dynamic contrast-enhanced imaging; Cerebral blood perfusion

1. Introduction

Dynamic contrast-enhanced (DCE) imaging with computed tomography (CT) or magnetic resonance imaging (MRI) is widely used in scientific research and clinical practice for in vivo assessment of the cerebral blood perfusion (Klotz and Konig, 1999; Koenig et al., 2001; Vonken et al., 1999; Wirestam et al., 2000). Increasing evidence has shown that the perfusion information derived from DCE imaging data can potentially be helpful to understand the pathophysiology of cerebral vascular diseases (Cala-mante et al., 2002; Koenig et al., 2001), and allows the clinicians to monitor and assess the therapeutic effects (Guckel et al., 1994; Koh et al., 2004).

In the technique of DCE imaging, an injection of contrast medium (tracer) is administrated intravenously, and then continuous acquisition of data from a single scan slice is performed. The passage of tracer particles through the brain creates the temporal changes of physical signals (amount of absorbed X-ray radiation in CT; local susceptibility in MRI), which in turn cause intensity changes on the captured sequential images. From those images, we can assess the changes in tracer concentration over time, which not only monitor the tracer kinetic behavior but also reflect the brain hemodynamic status. In clinical practice, DCE imaging normally acquires 50–100 images per case with a scan time of 1 s/frame or 0.5 s/frame. To extract

---

* Corresponding author. Address: Centre for Advanced Computations in Engineering Science, National University of Singapore, BLK EA-04-26, 10 Kent Ridge Crescent, Singapore 119260, Singapore.
 E-mail address: xingyewu@pmail.ntu.edu.sg (X.Y. Wu).

useful information from those image series and depict the underlying physiological process, a variety of image analysis techniques have been proposed and investigated.

1.1. Analysis of dynamic contrast-enhanced images

Simple parametric maps showing time to peak signal intensity and peak intensity values are commonly used, as they are easy to calculate and may have some relation to physiological parameters. However, they are also related to the rate of contrast injection and particular imaging sequences, hence cannot reliably measure the cerebral hemodynamics.

Alternatively, microcirculatory parameters, such as cerebral blood flow, cerebral blood volume, and mean transit time, have been increasingly reported, because they can eliminate the effect of injection rate, and are physiologically meaningful (Calamante et al., 2002; Koenig et al., 2001; Koh et al., 2004). The calculation of microcirculatory parameters is based on the indicator-dilution theory, which assumes a convolution integral relationship between the residual tracer concentration and the arterial input, and hence entails a deconvolution process (Koh and Hou, 2002; Koh et al., 2004; Wirestam et al., 2000). In practice, the arterial input function is usually estimated by sampling at a major artery (anterior or middle cerebral artery), and the sampling region is manually selected by experts with anatomy knowledge (Murase et al., 2001), which hence restricts the possibility of automatic analysis. In addition, to account for the time delay of tracer passage in cerebral tissue relative to the sampling artery, bolus arrive times (BATs) have to be estimated. Otherwise, the time delay could cause a significant bias in the estimated microcirculatory parameters (Calamante et al., 2000; Cheong et al., 2003). Although the calculation of the BAT using regression model is less than 20 ms (Cheong et al., 2003), it could take more than 20 min in a voxel-by-voxel analysis where tens of thousands of BATs need to be calculated. The requirement for computation of BATs limits the application of deconvolution techniques for quick analysis.

In this work, we investigate the use of independent component analysis (ICA) on DCE imaging data for assessment of cerebral blood perfusion, without any prior knowledge of the underlying tissue vasculature and arterial input function. ICA is a powerful data-driven statistical technique. It has been successfully used in the analysis of electroencephalographic (EEG) and magnetoencephalographic (MEG) recordings (Hyvarinen, 1999a). Recently, ICA has been applied in functional magnetic resonance imaging (fMRI) studies to extract the task-related brain activation (Beckmann and Smith, 2004; Calhoun et al., 2004; Jung et al., 2001; McKeown et al., 1998a; McKeown and Sejnowski, 1998b). We were, therefore, motivated to investigate the application of ICA on DCE imaging data for assessment of cerebral blood perfusion. In the literature, ICA has also found applications in DCE-MRI for hemodynamic segmentation of the brain (Kao et al.,

2003), development of MR angiography (Suzuki et al., 2003), and detection of the breast lesions (Yoo et al., 2002).

1.2. Independent component analysis

ICA was originally proposed to solve the blind source separation (BSS) problem (Comon, 1994). For DCE imaging, the measured data could be looked as a summation of the brain hemodynamic behaviors (caused by different local microvasculature and brain functional status) and some artificial processes (such as subtle head movements, physiological pulsations, and machine noise). By assuming the spatial independence of those hemodynamic patterns and artificial processes, the ICA technique is able to separate those mixed signals. As the areas affected by abnormal brain functions, for example, tumors, should be unrelated to those affected by artificial factors, ICA also has the potential to reveal brain hemodynamic abnormalities.

In the independent component analysis of DCE imaging data, each frame of the sequential images is converted into a 1D row signal vector, $\mathbf{X}_i \, (i = 1, \ldots, m)$, where i is the index of scan time point, and m is the total number of scans. The length of the signal vector, v, is equal to the number of voxels per frame. The signal $\mathbf{X}_i$ is considered as a linear combination of the independent components, $\mathbf{C}_j \, (j = 1, \ldots, n)$

$$X_{ik} = \sum_{j=1}^{n} M_{ij} \cdot C_{jk}, \quad (k = 1, \ldots, v). \tag{1}$$

The entire image data can be expressed as

$$\mathbf{X} = \mathbf{M} \cdot \mathbf{C}, \tag{2}$$

or in other form:

$$\mathbf{C} = \mathbf{W} \cdot \mathbf{X}, \tag{3}$$

where $\mathbf{X}$ is the $m \times v$ measured data matrix, $\mathbf{M}$ is the $m \times n$ mixing (linear combination) matrix, and $\mathbf{C}$ is the $n \times v$ component matrix. The $n \times m$ weight matrix, $\mathbf{W}$ (also called unmixing matrix), is the pseudo-inverse of $\mathbf{M}$. Both of the weight matrix and the component matrix can be obtained by iteratively updating the elements of $\mathbf{W}$ such that the target components $\mathbf{C}_j$ can meet some criteria (as independent to each other as possible). The raw vector $\mathbf{C}_j$ is then reformed into 2D to construct the component map. Those maps are fixed over time, while the relative contribution of each map changes with a unique associated time course (column of mixing matrix, $\mathbf{M}$).

Different algorithms for implementation of independent component analysis have been proposed, such as JADE (Cardoso and Souloumiac, 1993), Infomax (Bell and Sejnowski, 1995), FastICA (also called fixed-point ICA, Hyvarinen, 1999b) and Nonparametric ICA (Samarov and Tsybakov, 2004). The Infomax ICA and FastICA are often applied in the implementation of spatial ICA (Calhoun et al., 2004; Jung et al., 2001; Kao et al., 2003; McKeown et al., 1998a; Yoo et al., 2002). Although their general performances are near equally fine (Jung et al., 2001), the FastICA is superior in terms of computation load

(Giannakopoulos et al., 1999), while the Infomax ICA has advantages in global estimation and noise reduction (Esposito et al., 2002). Detailed comparison of these algorithms can be found in the literature (Cardoso, 1997; Calhoun et al., 2004; Esposito et al., 2002; Giannakopoulos et al., 1999; Hyvarinen et al., 2001). The Infomax ICA was employed in our work. This algorithm is based on the Infomax principle. It initializes $\mathbf{W}$ to the identity matrix $\mathbf{I}$, then iteratively attempts to maximize the joint entropy of the outputs passed through a set of nonlinear functions, $g(\cdot)$. The nonlinear function, which provides necessary higher-order statistical information, is chosen to be the logistic function:

$$g(\mathbf{C}_i) = \frac{1}{1 + e^{-\mathbf{C}_i}}, \quad (4)$$

where $\mathbf{C} = \mathbf{WZ} = \mathbf{WVX}$, $\mathbf{V} = 2(\mathbf{XX}^T)^{-1/2}$. The use of the whitening matrix $\mathbf{Z}$ instead of $\mathbf{X}$ aims to constrain the matrix $\mathbf{W}$ to be symmetric (Jung et al., 2001). The entropy in a discrete form is:

$$H(\cdot) = -\sum_k p_k \log p_k, \quad (5)$$

where p_k is the probability of the kth event. The elements of $\mathbf{W}$ are updated using small batches of data vectors drawn randomly from $\mathbf{Z}$ without substitution, according to:

$$\Delta \mathbf{W} = -\eta \left(\frac{\partial H(g(\mathbf{C}))}{\partial \mathbf{W}} \right) \mathbf{W}^T \mathbf{W} = \eta(I + \mathbf{YC}^T)\mathbf{W}, \quad (6)$$

where η is the learning rate (typically near 0.01, and is gradually reduced until $\mathbf{W}$ stops changing appreciably) and the vector $\mathbf{Y}$ has elements:

$$y_i = \frac{\partial}{\partial \mathbf{C}_i} \ln \left(\frac{\partial g(\mathbf{C}_i)}{\partial \mathbf{C}_i} \right) = 1 - 2g(\mathbf{C}_i). \quad (7)$$

More detailed discussion of the training process can be found in the literature (Bell and Sejnowski, 1995).

In this work, the Infomax ICA was applied to both synthetic data and real dynamic contrast-enhanced CT imaging data. In particular, we examined the performance of ICA to reveal cerebral vascular abnormalities and its applicability as a tool for clinical image analysis.

2. Methods

2.1. Simulation experiment

Totally 9 forms of simulated concentration–time curves were employed in the experiment. Those concentration–time curves were obtained from the DCE CT imaging data of a patient with a meningioma and cerebral ischemia. Smoothing preprocess was applied on those signals before constructing synthetic dynamic images. A synthetic brain mask was used to discriminate the location of each form of curves, as shown in Fig. 1a and b. Synthetic dynamic images consist of 50 images of 63×63 voxels with a time interval Δt of 1 s. Gaussian noise was then added to simulate noisy concentration–time curves with signal to noise ratios (SNRs) of 5, 10, 20 and 50. These SNR values are common in DCE imaging. The SNR is approximated by the ratio of standard deviation of the arterial signal to that of the noise. Similar to the previous work (Koh et al., 2004), a preprocessing step of smoothing with a 3×3 median kernel was applied to those synthetic images. The dimension of the synthetic data were reduced by preprocessing the data with PCA. The Infomax ICA scheme (McKeown et al., 1998a) was then used to separate the preprocessed synthetic images into independent spatial components. The simulation experiment was carried out in MATLAB on a Pentium IV personal computer.

2.2. Patient study

In this study, the real DCE-CT imaging data are the same as those in our previous work (Koh et al., 2004; Wu, 2004). Nine patients (3 females, 6 males), ages from
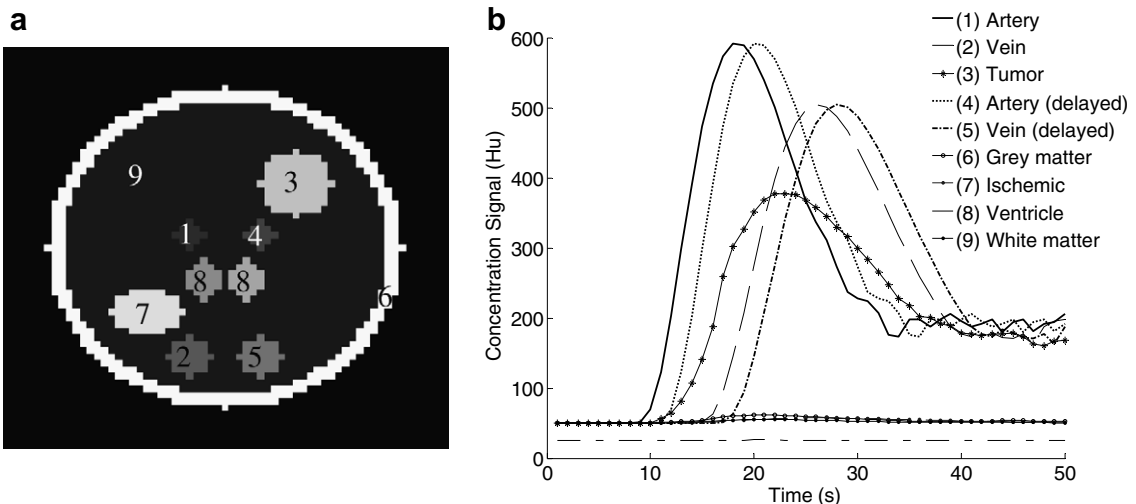

Fig. 1. (a) Synthetic brain mask. 1, artery; 2, vein; 3, tumor; 4, artery (2 s delayed); 5, vein (2 s delayed); 6, grey matter; 7, ischemic area; 8, ventricles; 9, white matter. (b) Concentration–time curves used in synthetic DCE imaging data.

55 to 81, with ischemia and/or brain tumor were involved. All the images were transferred to a Pentium IV personal computer for processing. The entire data analysis was implemented in MATLAB. For each patient, voxels outside the brain were excluded by a minimum signal threshold. PCA preprocessing was used to reduce the dimension of the data. The Infomax ICA scheme was then carried out to extract independent component maps and associated time courses.

2.3. Image analysis

The number of independent components (ICs), n, is the only parameter that needs to be determined before carrying out ICA. Although the exact number of ICs is always unknown in practice, the assumption that it is not more than the number of measured signals ($n \leqslant m$) is acceptable, and can make the problem more tractable. Different criteria, such as the Bayesian information criterion (BIC), the Akaike information criterion (AIC), the minimum description length (MDL) criterion, and their modified versions have been used in image analysis for model order selection (Beckmann and Smith, 2004; Calhoun et al., 2001). In this study, we estimated the number of ICs by using the MDL criterion. MDL was originally proposed by Rissanen (1978) and then popularized in the signal processing community by Wax and Kailath (1985). The MDL criterion has been found unbiased and statistically consistent (Wax and Kailath, 1985). For our case, MDL has the form as

$$
\begin{aligned}
\mathrm{MDL}(k) = {} & -(m-k) \cdot v \cdot \ln \frac{\prod_{i=k+1}^{m} \lambda_i^{1/(m-k)}}{\frac{1}{m-k} \sum_{i=k+1}^{m} \lambda_i} \\
& + \frac{1}{2} k \cdot \left(m - \frac{k-1}{2} \right) \cdot \ln v,
\end{aligned}
\tag{8}
$$

where k is the number of ICs (sources), m is the total number of scans, v is the number of voxels per frame, and λ_i denotes the ith largest eigenvalue of the covariance matrix, $\mathbf{X}\mathbf{X}^{\mathrm{T}}$. The estimation of the number of ICs is determined as the value of $k \in \{1, \ldots, m-1\}$ for which the corresponding MDL value is minimized.

After obtaining a few independent spatial components by ICA, a problem has to be dealt with is how to identify a ''meaningful'' subset from the component set, because a large majority of components are non-interesting (noise or uninterpretable component). The kurtosis of components' distribution of voxel values could be useful for this issue (Arfanakis et al., 2002; Formisano et al., 2002), because components with a kurtosis near zero (Gaussian distribution) are more likely to present a noise-like spatial distribution than recognized spatial patterns. In this study, a simple oscillatory index was employed to select the components of interest. The basic idea lies in the fact that the cerebral hemodynamic patterns should have relatively smooth time courses, while the noise component could be

very unpredictable and always presents an oscillatory time course. Therefore, we may consider the components with smoother time courses as the components of interest. By simply estimating the smoothness of all the time courses, we can select the components of interest from the whole component set. The smoothness is estimated by the oscillatory index, O_i, which is defined as:

$$
O_i = \frac{\sum_j |M_{j+1,i} - M_{j,i}|}{\max(\mathbf{M}_i) - \min(\mathbf{M}_i)},
\tag{9}
$$

where $\mathbf{M}_i$ is the ith column of the mixing matrix (the time course of the ith component), and $M_{j,i}$ is the element of the jth row and ith column. Those time courses are considered significantly smooth, if the following criterion is met:

$$
O_i \leqslant \bar{O} - l \cdot \mathrm{SD},
$$

where $\bar{O}$ and SD represent the mean value and standard deviation of the oscillatory indices, respectively. The value of l is used to tune the threshold. Alternatively, we can simply select a fixed number of components associated with the smallest oscillatory indices. In order to keep as many components of interest as possible, we experientially choose $l = 1.28$ in our patient study experiments, and select seven components with the smallest oscillatory indices in the simulation experiment.

In order to make comparison, the generated independent component maps were converted to Z scores and thresholded. The Z scores do not have determinate statistical meanings (McKeown et al., 1998a), but were used to describe areas (voxels with $z \geqslant 3.5$) that contribute largely to a particular component. Those areas were compared with the synthetic brain mask using the similarity rate (SR), which is defined as:

$$
\mathrm{SR} = \frac{\text{the number of same significant voxels}}{\text{average number of significant voxels}}.
\tag{10}
$$

3. Results

3.1. Simulation results

The thresholded Z maps ($z \geqslant 3.5$) of interpretable ICs (generated by the Infomax ICA scheme with SNR = 50, the number of ICs = 13) were combined into one binary map, as shown in Fig. 2a. The corresponding time courses were shown in Fig. 2b. The tumor, artery, vein and ventricle areas in the binary map match with the synthetic brain mask in terms of both shape and position. The corresponding contribution–time curves also show consistency with related concentration–time curves. However, we also note that the ICA scheme failed to reveal ischemia, white matter and gray matter areas in our simulation, and the successfully revealed areas shrink a little. The contribution–time curve of the artery (delayed) related component decreases compared with the original concentration–time curve. In addition, part of the artery (delayed) region also contrib-
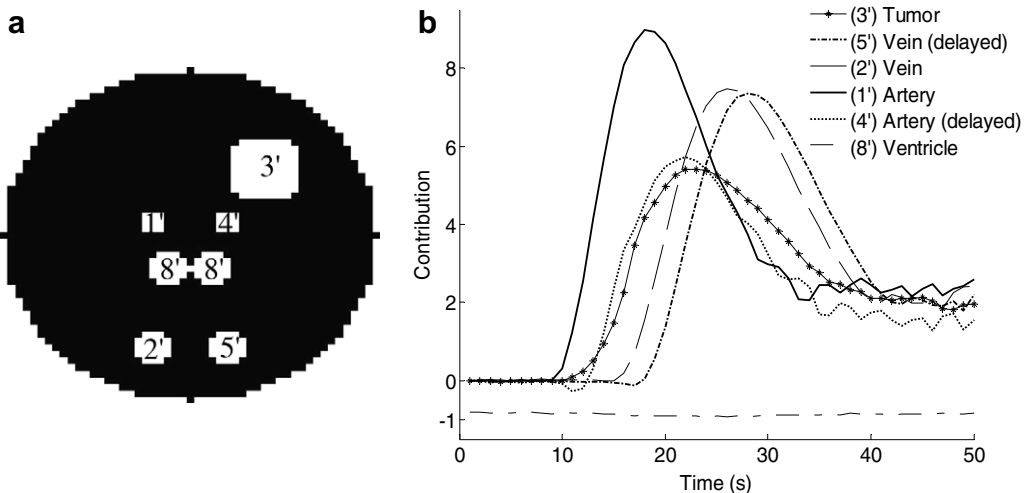
Fig. 2. (a) Combined binary map of interpretable independent components and (b) their corresponding time courses. The MDL criterion suggests the number of ICs to be 13 at the noise level of SNR = 50. The Infomax ICA successfully separates the tumor (3′), artery (1′, 4′), vein (2′, 5′) and ventricle (8′) related components, while the grey matter, white matter and ischemic areas are not revealed.

Table 1
Similarity rates (%) of the areas that contribute largely to the respective interpretable ICs compared with the original synthetic brain mask at various SNRs and number of ICs

SNR	Number of ICs	SR (%) in the respective areas					
		Tumor	Artery	Artery (delayed)	Vein	Vein (delayed)	Ventricle
5	50	87.50	81.82	NA	84.00	59.15	NA
	20	87.50	75.00	NA	75.00	59.15	9.01
	11[a]	87.50	69.23	NA	72.41	59.15	11.01
	5	87.50	54.55	NA	72.41	59.15	10.91
10	50	87.50	58.06	NA	84.00	59.15	IC splits
	20	87.50	60.00	75.00	84.00	59.15	74.47
	13[a]	87.50	60.00	78.26	80.77	59.15	74.47
	5	87.50	58.06	NA	71.19	59.15	71.11
20	50	92.22	81.82	58.06	IC splits	84.00	90.32
	20	92.22	58.06	81.82	84.00	84.00	90.32
	13[a]	92.22	58.06	81.82	84.00	84.00	90.32
	5	92.22	58.06	NA	71.19	84.00	86.60
50	50	96.25	81.82	81.82	84.00	84.00	IC splits
	20	92.22	81.82	81.82	84.00	84.00	90.32
	13[a]	92.22	81.82	81.82	84.00	84.00	90.32
	5	92.22	58.06	NA	71.19	84.00	85.71

[a] Number of independent components suggested by the MDL criterion.

utes to the component that is highly correlated to the tumor (not shown).

The interpretable independent component maps do not change abruptly when the number of ICs decreases. The respective similarity rates compared with original synthetic brain mask are shown in Table 1. However, we note when the number of ICs is set as large as 50, the generated component splits severely. One example is shown in Fig. 3. In this case (SNR = 50, the number of ICs = 50) the ventricle related component is split into two. The areas that contribute largely to the respective components almost have the same shape and position (Fig. 3, left) in the map, while

their corresponding time courses (Fig. 3, right) show complementary properties. On the contrary, when the number of ICs is set too small, some of the patterns cannot be separated (rows 10, 14 and 18 in Table 1).

The MDL criterion suggests a moderate number of ICs in our simulation (Table 1). Although it is a little overestimating (the actual number of source signals is 10 including noise), the obtained component maps and corresponding time courses are acceptable. Furthermore, reducing the dimension of the data with MDL and PCA can save the computation time of ICA from around one hundred seconds to ten. Most of the interpretable independent
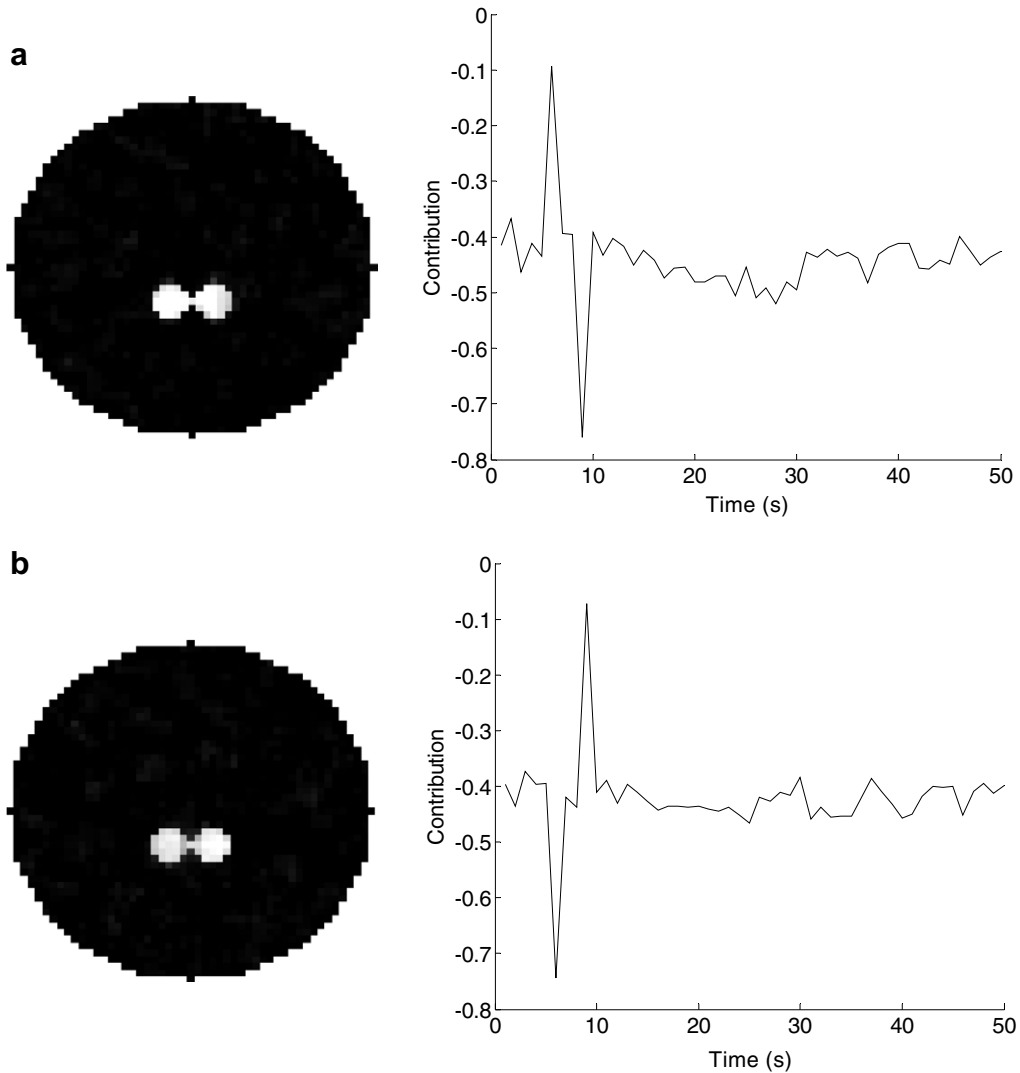
Fig. 3. Example of component splitting (SNR = 50, the number of ICs = 50). The ventricle related component was split into two (a) and (b). The areas that contribute largely to the respective components almost have the same shape and position (left), while their corresponding time courses (right) show complementary properties.

components are within the selected subset using the oscillating index method, except some cases when the components split severely (due to the large number of ICs). The calculation of oscillatory indices is within 1 ms.

3.2. Patient case results

Four representative study cases are shown here to illustrate the performance of ICA for revealing cerebral vascular abnormalities. In the case study of a patient with two tumors, 31 (suggested by MDL criterion) independent component maps and corresponding time courses were generated by the Infomax ICA. Among them, five components were automatically selected based on the oscillatory indices. All the components of interest were found within the selected component set. The component maps and their corresponding time courses are shown in Fig. 4. In order to make comparison, the respective contribution–

time curve (solid line) and the real tracer concentration–time (TC) curve (dash line, obtained from one voxel of the region of interest) were plotted together. The maximum amplitude of each curve was normalized to unit 1 for display. Fig. 4a shows a component representing the arterial pattern. The component map (Fig. 4a, left) presents the arterial structure clearly, and its contribution–time curve shows consistency with the real arterial TC curve (Fig. 4a, right). Fig. 4b demonstrates the venous pattern. Besides the above two, one component that is highly correlated to the brain tumors was also extracted (Fig. 4c). The location and the shape of the tumors can be clearly identified in the component map. The corresponding contribution–time curve shows similarity with the real TC curve.

The ICA results of a patient with metastases from the lungs are shown in Fig. 5. The number of ICs was set to 36 according to the MDL criterion. In this case, the struc-
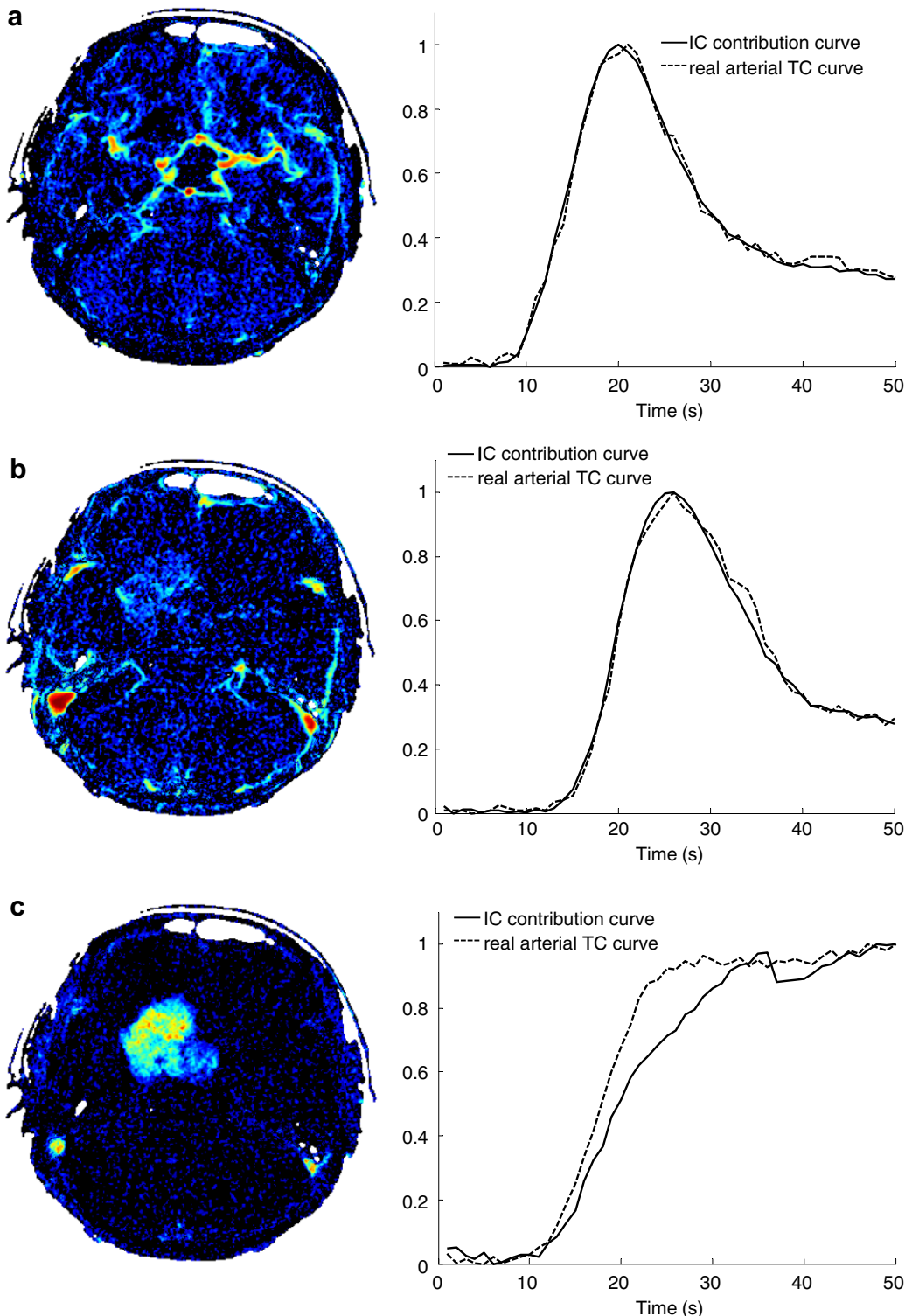
Fig. 4. Case study of a patient with tumors using the Infomax ICA. Both of the independent component maps (left) and the corresponding time courses (right, solid line) are shown. In order to make comparison, the contribution curve and the real tracer concentration–time curve (dashed line) were plotted together. The maximum amplitude of each curve was normalized to unit 1 for display. (a) Arterial pattern. (b) Venous pattern. (c) Tumorous pattern.

ture of the artery and vein, especially the sagittal sinus, is clearly observed (Fig. 5a, b, left). The two metastatic tumors are also obvious in the corresponding component map. After the radiotherapy treatment, the tumor related

component map (Fig. 6, the number of ICs was set to 39) of the same patient shows an obvious reduction in the tumor extent, which illustrates a positive effect of the treatment. The corresponding contribution–time curve presents
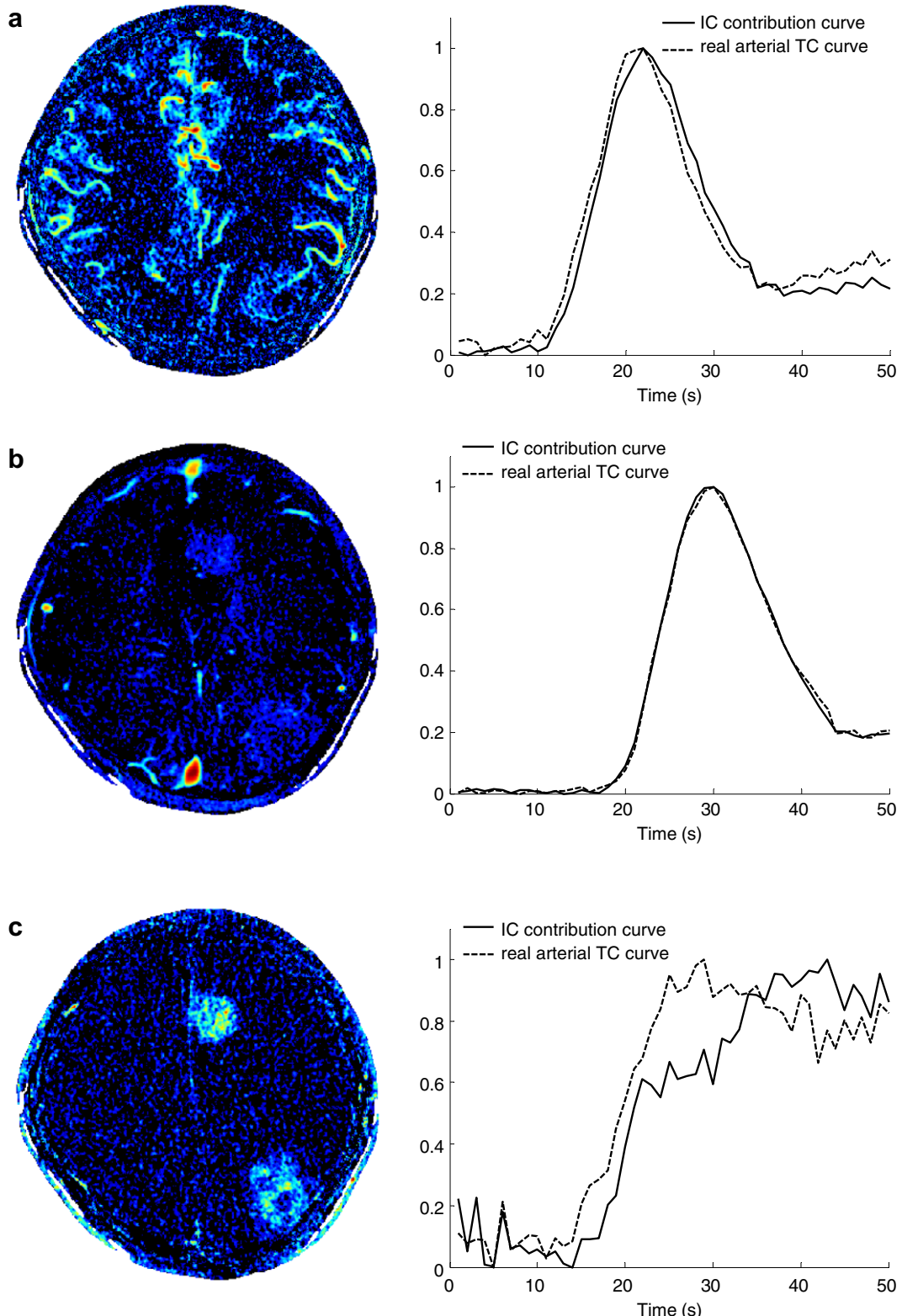
Fig. 5. Case study of a patient with metastases from the lungs before radiotherapy using the Infomax ICA. The independent component maps are shown in the left. The corresponding contribution–time curves (solid line) and real tracer concentration–time curves (dashed line) are shown in the right. (a) Arterial pattern. (b) Venous pattern. (c) Tumorous pattern.

a shift from the real TC curve. The sagittal sinus area is observed in the tumor related component map (Fig. 6, arrow).

The case study of a patient with ischemia was also carried out. Although ICA (the number of ICs was set to 37) failed to extract a component that is highly correlated to the
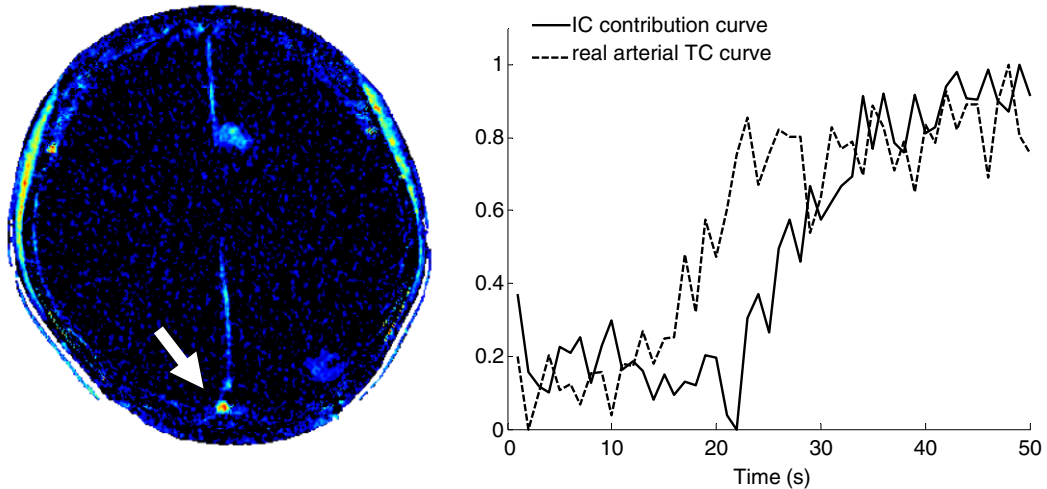
Fig. 6. The same patient as in Fig. 5, after radiotherapy. The tumor related independent component map is shown in the left. The corresponding contribution–time curve (solid line) and real tracer concentration–time curve (dashed line) are shown in the right. The sagittal sinus area is also observed in the component map (arrow).
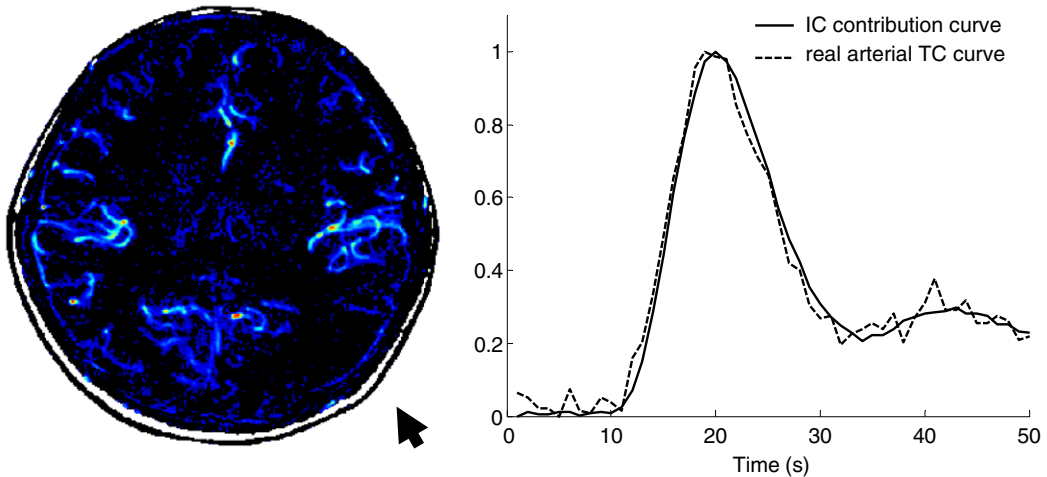

Fig. 7. Case study of a patient with ischemia using the Infomax ICA. The artery related independent component map is shown in the left. The corresponding contribution–time curve (solid line) and real tracer concentration–time curve (dashed line) are shown in the right. The component map shows reduced intensity in the left occipital lobe (arrow).

ischemia, the infarction is still recognizable in the artery related component map as shown in Fig. 7. The ischemic territory can be observed in the left occipital lobe (Fig. 7, arrow), with reduced intensity compared to its mirror area.

In all the study cases, components that are highly correlated to arterial patterns as well as venous patterns were obtained. In seven out of nine tumor cases, the components that represent tumorous patterns were successfully extracted. In the rest two cases, the tumor territories are recognizable in the vein related component maps.

4. Discussion

4.1. Simulation study

This simulation result illustrates the capability of the ICA technique to separate different brain hemodynamic patterns. After the dimension of the data is reduced by PCA according to the MDL criterion, the ICA scheme performs well in terms of both reliability and efficiency. In fact, the PCA preprocessing diminishes the noise effect to some extent, which hence improves the ICA result (Hyvarinen, 1999a). Part of the artery region was found contributing largely to the tumor related component map. This kind of components overlapping is possible, because one voxel might contribute significantly (at different level) in more than one component maps when the corresponding time courses are similar. The interpretable independent component maps do not show abrupt changes when the number of ICs decreases. This is possibly because a large percentage of the total variance of the data was remained in the PCA preprocessing step, therefore components with large changes in time courses (contribute most of the data variance), such as artery, vein and tumor related components

could be essentially unchanged. In the simulation, other sources (ischemia, grey matter and white matter) that contribute less to the data variance were not separated. They might be either corrupted by noise or ruined in component splitting. In addition, the information about those sources may be discarded during the PCA preprocessing step, because they are corresponding to small eigenvalues. One way to solve this problem might be removing the recognizable components and run ICA iteratively (Kao et al., 2003).

The MDL criterion suggests a consistent number of ICs in our simulation. Although it is a little overestimating, the ICA results were not badly affected. Actually, the exact number of ICs is always unknown and difficult to estimate in practice. For simplicity, we may assume $n = m$, so that we can get a square mixing matrix. However, m is determined by the image acquisition scheme (number of scans in DCE imaging) that has little relationship to the number of independent sources in the brain. Choosing the number of ICs heuristically is also not a good option, as it needs more prior knowledge and can result in an arbitrary threshold level. McKeown and Sejnowski (1998b) suggested that the number of ICs can be reduced by first preprocessing the data with the PCA technique, which provides a way of keeping the advantage of a square mixing matrix without having $n = m$. Nevertheless, the cutoff point for the eigenvalues may not be obvious, and improper choice takes a risk of changing the intrinsic dimensionality and leads to a suboptimal results (Esposito et al., 2002). On the one hand, underestimation of the data dimensionality will discard too much valuable information and result in poor performance of component extraction. On the other hand, overestimation will highly increase the computational cost and raise the risk of component splitting. An easy way to determine the cutoff point might be using the simplistic criteria like retaining 99% of eigenvalues. This method can eliminate some of the noise effect but still has no relation to the problem of correctly estimating the number of independent sources. From this point of view, the MDL criterion at least provides a way to estimate the number of ICs.

The oscillating index method shows a good performance for automatically selecting the components of interest, as long as the number of ICs is properly set. Compared with other selection criterion, such as kurtosis of the components' distribution of voxel values, the oscillating index method provides the advantage of computational simplicity.

4.2. Patient study

From the patient case studies, we note that independent component analysis has the capability to extract components that represent cerebral hemodynamic patterns from the DCE imaging data. The main advantage of ICA is that it makes little prior assumption about the underlying physiology and allows the intrinsic structure of the clinical data to be accessed. This can be very important for patients with complex cerebral hemodynamic patterns.

Another advantage of ICA is that the obtained independent component maps have good clarity. The arterial and venous structures can be identified readily. Furthermore, as the tumor related component is separated from the arterial and venous components, it allows better demarcation of the tumor territories compared with conventional microcirculatory parametric maps.

In addition, ICA can provide both spatial information and temporal information, because both independent component maps and their corresponding time courses can be achieved. Therefore, ICA can be helpful to understand cerebral hemodynamics and make clinical diagnosis. Although the contribution–time curves cannot be interpreted as tracer concentration–time curves directly (they were rescaled during the ICA process), they do show similarity with the real TC curves after both being normalized.

The computational efficiency is also an advantage of ICA. In our study, the total process time for one patient with the Infomax ICA is about 6 min, less than half of the time needed for numerical deconvolution. Furthermore, neither the manually selected arterial input function nor the calculation of bolus arrive times is required for ICA, while both of them are needed for deconvolution analysis.

In our study, the number of independent components suggested by MDL criterion might be a little overestimated as it is fairly larger than the number of selected components of interest. However, considering the complexity of patients' cerebral hemodynamics and the unknown noise factors, we do not advise using a very small number of independent components. Recently, Li et al. (2006) have proposed a correction method for order selection to deal with the over-estimation problem.

Normally 4–6 components of interest were automatically selected using the oscillating index method ($l = 1.28$). Besides the arterial, venous and tumorous components, some components that may suggest head movements were also observed. In Fig. 8, the ring-like pattern in the component map (left) together with the corresponding monotonic contribution–time curve (right) may represent a slow head shift. In Fig. 9, there was a sudden drop on the corresponding time course, which may be caused by a small quick head movement. Similar components that are highly correlated to head movements were also reported in other applications (McKeown and Sejnowski, 1998b). If such head movements can be confirmed, those components could be helpful to eliminate or reduce the effect of head movements. From this point of view, ICA can be used as a preprocessing step prior to further analysis by other techniques.

In conclusion, ICA has the capability to separate the DCE imaging data into physiologically meaningful components, which present qualitative information about the cerebral blood perfusion. The obtained artery and vein related components can provide reliable reference to identify the arterial and venous structure. The tumorous component map allows better demarcation of the tumor territories compared with conventional microcirculatory
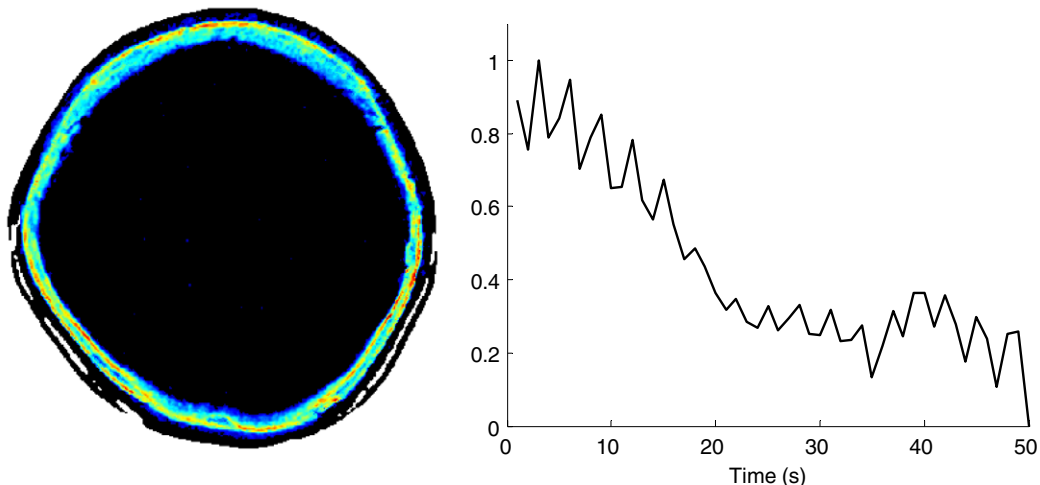
Fig. 8. Case study of a patient with metastases from the lungs before radiotherapy using the Infomax ICA. The independent component map (left) and corresponding time course may suggest a gradual head movement.
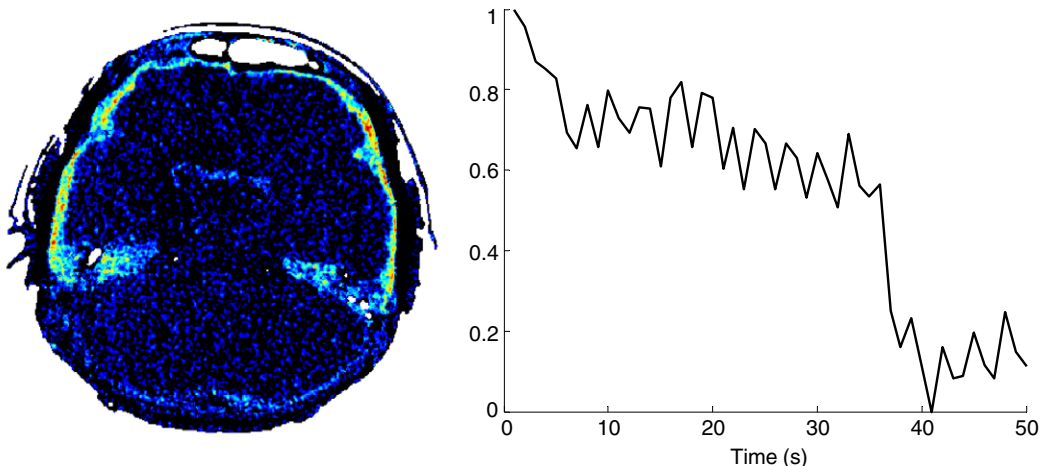

Fig. 9. Case study of a patient with tumors using the Infomax ICA. The independent component map (left) and corresponding time course may suggest a quick head movement.

parametric maps. Reducing the dimension of the clinical data by PCA and MDL can make ICA work more efficiently. The components of interest can be automatically selected using the simple oscillating index method. Our study has demonstrated that ICA has the potential to be a useful clinical tool for diagnosis of cerebral tumors and ischemic stroke, as well as the assessment of treatment response. However, the patient cases in our study are limited, further validation work needs to be carried out.

Acknowledgements

References

Arfanakis, K., Cordes, D., Haughton, V.M., Carew, J.D., Meyerand, M.E., 2002. Independent component analysis applied to diffusion tensor MRI. Magn. Reson. Med. 47, 354–363.

Beckmann, C.F., Smith, S.M., 2004. Probabilistic independent component analysis for functional magnetic resonance imaging. IEEE. Trans. Med. Imaging 23 (2), 137–152.

Bell, A.J., Sejnowski, T.J., 1995. An information-maximization approach to blind separation and blind deconvolution. Neural Comput. 7, 1129–1159.

Calamante, F., Gadian, D.G., Connelly, A., 2000. Delay and dispersion effects in dynamic susceptibility contrast MRI: simulations using singular value decomposition. Magn. Reson. Med. 44, 466–473.

Calamante, F., Gadian, D.G., Connelly, A., 2002. Quantification of perfusion using bolus tracking magnetic resonance imaging in stroke:

assumptions, imitations, and potential implications for clinical use. Stroke 33 (4), 1146–1151.

Calhoun, V.D., Adali, T., Pearlson, G.D., Pekar, J.J., 2001. A method for making group inferences from functional MRI data using independent component analysis. Hum. Brain Mapp. 14, 140–151.

Calhoun, V., Pearlson, G., Adali, T., 2004. Independent component analysis applied to fMRI data: a generative model for validating results. J. VLSI Signal Process. 37, 281–291.

Cardoso, J-F., Souloumiac, A., 1993. Blind beamforming for non Gaussian signals. IEEE Proceedings-F. 140, 362–370.

Cardoso, J.-F., 1997. Infomax and maximum likelihood for blind source separation. IEEE Signal Process. Lett. 4 (4), 112–114.

Cheong, L.H., Koh, T.S., Hou, Z., 2003. An automatic approach for estimating bolus arrival time in dynamic contrast MRI using piecewise continuous regression models. Phys. Med. Biol. 48, N83–N88.

Comon, P., 1994. Independent component analysis, a new concept? Signal Process. 36, 287–314.

Esposito, F., Formisano, E., Seifritz, E., Goebel, R., Morrone, R., Tedeschi, G., Salle, F.D., 2002. Spatial independent component analysis of functional MRI time-series: to what extent do results depend on the algorithm used? Hum. Brain Mapp. 16, 146–157.

Formisano, E., Esposito, F., Kriegeskorte, N., Tedeschi, G., Salle, F.D., Goebel, R., 2002. Spatial independent component analysis of functional magnetic resonance imaging time-series: characterization of the cortical components. Neurocomputing 49, 241–254.

Giannakopoulos, X., Karhunen, J., Oja, E., 1999. An experimental comparison of neural algorithms for independent component analysis and blind separation. Int. J. Neural Syst. 9 (2), 99–114.

Guckel, F., Brix, G., Rempp, K., Deimling, M., Rother, J., Georgi, M., 1994. Assessment of cerebral blood-volume with dynamic susceptibility contrast-enhanced gradient-echo imaging. J. Comput. Assist. Tomo. 18 (3), 344–351.

Hyvarinen, A., 1999a. Survey on independent component analysis. Neural Comput. Surv. 2, 94–128.

Hyvarinen, A., 1999b. Fast and robust fixed-point algorithms for independent component analysis. IEEE Trans. Neural Networks 3, 626–634.

Hyvarinen, A., Karhunen, J., Oja, E., 2001. Independent Component Analysis. Wiley-Interscience.

Jung, T.-P., Makeig, S., McKeown, M.J., Bell, A.J., Lee, T.-W., Sejnowski, T.J., 2001. Imaging brain dynamics using independent component analysis. Proc. IEEE 89 (7), 1107–1122.

Kao, Y.-H., Guo, W.-Y., Wu, Y.-T., Liu, K.-C., Chai, W.-Y., Lin, C.-Y., Hwang, Y.-S., Liou, A.J.-K., Wu, H.-M., Cheng, H.-C., Yeh, T.-C., Hsieh, J.-C., Teng, M.M.H., 2003. Hemodynamic segmentation of MR brain perfusion images using independent component analysis, thresholding, and Bayesian estimation. Magn. Reson. Med. 49, 885–894.

Klotz, E., Konig, M., 1999. Perfusion measurements of the brain: using dynamic CT for the quantitative assessment of cerebral ischemia in acute stroke. Eur. J. Radiol. 30, 170–184.

Koenig, M., Kraus, M., Theek, C., Klotz, E., Gehlen, W., Heuser, L., 2001. Quantitative assessment of the ischemic brain by means of perfusion-related parameters derived from perfusion CT. Stroke 32, 431–437.

Koh, T.S., Hou, Z., 2002. A numerical method for estimating blood flow by dynamic functional imaging. Med. Eng. Phys. 24, 151–158.

Koh, T.S., Wu, X.Y., Cheong, L.H., Lim, C.C.T., 2004. Assessment of perfusion by dynamic contrast-enhanced imaging using a deconvolution approach based on regression and singular value decomposition. IEEE Trans. Med. Imaging 23 (12), 1532–1542.

Li, Y., Adali, T., Calhoun, V.D., 2006. Sample dependence correction for order selection in fMRI analysis. Proc. ISBI, 1072–1075.

McKeown, M.J., Makeig, S., Brown, G.G., Jung, T-P., Kindermann, S.S., Bell, A.J., Sejnowski, T.J., 1998a. Analysis of fMRI data by blind separation into independent spatial components. Hum. Brain Mapp. 6, 160–188.

McKeown, M.J., Sejnowski, T.J., 1998b. Independent component analysis of fMRI data: examining the assumptions. Hum. Brain Mapp. 6, 368–372.

Murase, K., Shinohara, M., Yamazaki, Y., 2001. Accuracy of deconvolution analysis based on singular value decomposition for quantification of cerebral blood flow using dynamic susceptibility contrast-enhanced magnetic resonance imaging. Phys. Med. Biol. 46, 3147–3159.

Rissanen, J., 1978. Modeling by shortest data description. Automatica 14, 465–471.

Samarov, A., Tsybakov, A., 2004. Nonparametric independent component analysis. Bernoulli 10 (4), 565–582.

Suzuki, K., Matsuzawa, H., Igarashi, H., Watanabe, M., Nakayama, N., Kwee, I.L., Nakada, T., 2003. All-phase MR angiography using independent component analysis of dynamic contrast enhanced MRI time series: -MRA. Magn. Reson. Med. Sci. 2 (1), 23–27.

Vonken, E.P.A., Van Osch, M.J.P., Bakker, C.J.G., Viergever, M.A., 1999. Measurement of cerebral perfusion with dual-echo multi-slice quantitative dynamic susceptibility contrast MRI. J. Magn. Reson. Imaging 10, 109–117.

Wax, M., Kailath, T., 1985. Detection of signals by information theoretic criteria. IEEE Trans. Acous. Sp. Sig. Proc. 33 (2), 387–392.

Wirestam, R., Andersson, L., Ostergaard, L., Bolling, M., Aunola, J.P., Lindgren, A., Geijer, B., Holtas, S., Stahlberg, F., 2000. Assessment of regional cerebral blood flow by dynamic susceptibility contrast MRI using different deconvolution techniques. Magn. Reson. Med. 43, 691–700.

Wu, X.Y., 2004. Functional neuroimaging and analysis. MEng Thesis, Nanyang Technological University, Singapore.

Yoo, S.-S., Choi, B.G., Han, J.-Y., Kim, H.H., 2002. Independent component analysis for the examination of dynamic contrast-enhanced breast magnetic resonance imaging data, Preliminary study. Invest. Radiol. 37 (12), 647–654.